Available online at www.sciencedirect.com
SCIENCE DIRECT
International Journal of Pharmaceutics 313 (2006) 114–122
INTERNATIONAL JOURNAL OF PHARMACEUTICS
www.elsevier.com/locate/ijpharm

# Experimental determination of the diffusion boundary layer width of micron and submicron particles

C. Galli *

*Pfizer Global Research and Development, 2800 Plymouth Road, Ann Arbor, MI 48105, United States*

Received 11 July 2005; received in revised form 31 December 2005; accepted 20 January 2006
Available online 9 March 2006

**Abstract**

Powder dissolution kinetics have shown that for particles in the so called "large" size regime (more than about 50 μm), the dissolution rate scales as the specific surface area, i.e. rate proportional to $d^{-1}$ where $d$ is the particle diameter. This is consistent with an effective diffusion boundary layer width $h_{EFF}$ that is constant with respect to particle size. However, for particles in the so called "small" size regime ($d$ less than about 50 μm), the dissolution rate has a stronger dependence than proportional to $d^{-1}$ [Bisrat, M., Anderberg, E.K., Barnett, M.I., Nystroem, C., 1992. Physicochemical aspects of drug release. XV. Investigation of diffusional transport in dissolution of suspended, sparingly soluble drugs. Int. J. Pharm., 80, 191–201; Mosharraf, M., Nystroem, C., 1995. The effect of particle size and shape on the surface specific dissolution rate of microsized practically insoluble drugs. Int. J. Pharm., 122, 35–47]. In this regime, Prandtl boundary layer theory predicts an $h_{EFF}$ approximately equal to the particle radius or diameter. This paper presents the first experimental determination of $h_{EFF}$ for particles less than about 2 μm. The powder dissolution kinetics of six suspensions over the particle diameter range of $5.9 \pm 0.1$ to $0.53 \pm 0.05$ μm are analyzed to yield $h_{EFF}$ values of $8.5 \pm 1.9$ to $0.34 \pm 0.14$ μm. The theoretical expectation for mass transport, dissolution time proportional to $d^{2.0}$, is in good agreement with the experimental results of dissolution time proportional to $d^{2.3}$. An understanding of these mass transfer mechanisms allows pharmaceutical scientists to achieve targeted release rates with minimum ensemble instability.


*Keywords:* Hydrodynamic boundary layer; Nanoparticles; Powder dissolution; Solubility limited; Prandtl boundary layer theory; Diffusion limited

## 1. Introduction

Understanding mass transfer mechanisms at solid–liquid interfaces is central to the design, control, and performance of numerous processes important in the pharmaceutical industry, including chemical crystallizations to synthesize drug substances, and "decrystallization" processes such as in vivo dissolution following bioadministration. As the modern pharmaceutical industry develops microvolume control of wet processes via arrested precipitation, impinging jet crystallization, and nanoparticle formation (Liversidge and Cundy, 1995; Grau et al., 2000; Muller et al., 2001; Merisko-Liversidge et al., 2003; Rasenack and Mueller, 2005; Vaughn et al., 2005), the length scale of required models decreases into the submicron region and below. For rational design of pharmaceutical formulations and processes, a thorough understanding of mass transport mechanics and associated transport distances is essential.

Mass transport between particulate and fluid phases is largely an expression of the spatial distribution of fluid momenta surrounding the solid particle. While a solid suspended in a liquid may be gaining mass via ripening, crystallization, or precipitation, maintaining mass if in phase equilibrium, or losing mass via dissolution, dispersions under agitation have similar interfacial structure. A fluid velocity gradient exists along the solid normal, with the maximum value, the free stream velocity, far from the interfacial region. For particles in the no slip limit, the velocity gradient decreases to a minimum near zero at the solid "wall" (Schlichting, 1955; Bird et al., 1960). Within this hydrodynamic boundary layer formed by the velocity gradient, there is a region along the solid–liquid wall where the fluid velocity is sufficiently low such that mass transfer is dominated by diffusion (Schlichting, 1955; Grijseels et al., 1981). It is this latter region, the "stagnant film" or effective diffusion boundary layer $h_{EFF}$, which is the subject of this paper.

* Present address: TransForm Pharmaceuticals, Inc., 29 Hartwell Avenue Lexington, MA 02421, United States. Tel.: +1 781 674 7863; fax: +1 781 863 7247.
*E-mail address:* cgalli@transformpharma.com.

0378-5173/$ – see front matter © 2006 Elsevier B.V. All rights reserved.
doi:10.1016/j.ijpharm.2006.01.030

Powder dissolution is a sensitive probe of both *interfacial* properties such as mass transfer rates across solid–liquid interfaces (Niebergall et al., 1963; Bisrat et al., 1992; Mosharraf and Nystroem, 1995) and *static* powder properties such as particle size and area (Hintz and Johnson, 1989), particle morphology (Kitamori and Iga, 1978; Lu et al., 1993; Dali and Carstensen, 1998), crystallinity/amorphous content (Hendriksen, 1990), and redispersibility (Galli et al., 2005). In the large particle regime of about 50 μm and above, the dissolution rate for a diffusion controlled process is proportional to the interfacial surface area: because the specific surface area is inversely proportional to diameter, the powder dissolution rate is proportional to $d^{-1}$, where $d$ is the particle diameter (Niebergall et al., 1963). However, powder dissolution kinetics have shown that for particles size less than about 50 μm, the dissolution rate increases more sharply than $d^{-1}$ (Bisrat et al., 1992; Mosharraf and Nystroem, 1995). This increased dependence of dissolution rate on diameter is typically ascribed to a decrease in the interfacial structure supported by small versus large particles. In the large particle regime, the effective diffusion boundary layer $h_{EFF}$ is constant with respect to particle size, and typically about 30 μm (Hintz and Johnson, 1989). This value can be determined for a specific powder by modeling intrinsic dissolution results (Carstensen, 1977). Particles of diameter less than 50 μm, however, do not have sufficient surface area and associated frictive force to support a hydrodynamic boundary layer and diffusion boundary layer of this magnitude. Prandtl boundary layer theory has postulated that for particles less than 50 μm, the effective hydrodynamic boundary layer $h_{EFF}$ is approximately equal to the particle radius or diameter (Schlichting, 1955; Niebergall et al., 1963; Mosharraf and Nystroem, 1995; Muller and Peters, 1998). It is worth noting that all drug powders go through this particle regime during the course of biodissolution.

The work described herein is the use of powder dissolution to determine the effective hydrodynamic boundary layer $h_{EFF}$ as a function of particle size over the diameter range of approximately 6–0.5 μm. After demonstrating that the powder dissolution data is recording a mass transfer process that is diffusion limited, a diffusion equation containing $h_{EFF}$ and the mass transfer rate $\dot{\mu}$ is introduced. This expression is then evaluated for $h_{EFF}$. The paper concludes with a short description of how this data can be used to target p$K$ profiles via API size control.

## 2. Materials and methods

### 2.1. Suspension preparation, particle size distributions and surface area

The suspensions for this study were formed via ultrahigh pressure homogenization (Galli et al., 2005). The size reduction system and process are currently under review by both United States and international patent offices. A suspension series of decreasing particle size was obtained by sampling the homogenizer as a function of process time; this series was labelled suspensions A through F. The particle size distribution and surface area of the suspensions were determined by differential centrifugal sedimentation (CPS Instruments, Inc; DC18000)(Fitzpatrick, 1999). The spin fluid was a sucrose density gradient ranging from 0% to 10% by weight; a typical rotational frequency was 12,000 rpm, resulting in a run time of 8 min. The solid concentration in the suspension and the injection volume were controlled to ensure linearity and accuracy with respect to the experimental results of total mass and volume detected; four to seven injections of 50–200 μL were recorded for each suspension. The true density of the drug powder was determined via helium pyncnometry (Quantichrome Ultrapycnometer 1000).

The specific surface area of the solid material in the suspension was also measured via differential centrifugal sedimentation. The specific surface area for each differential centrifugal sedimentation injection was calculated by dividing the total surface area detected by the total mass detected.

### 2.2. Powder solubility

To determine the powder solubility, the suspension series A through F was incubated on a platform shaker at 37 °C for at least 24 h. Aliquots of the suspensions were clarified at 37 °C via 1 h ultracentifugation at 4.7e6 × $g$. The supernatants were collected; precipitation was quenched via 1:1 dilution with 50:50 water:methanol. Four to six trials were completed for each suspension. The resulting solutions were chemically analyzed for drug and degradates via HPLC. Two ensemble methods were also used as referee methods. After 24 h incubation on a platform shaker at 37 °C, the saturated suspension A was transferred to a 1 cm quartz cuvette, and maintained at the desired temperature (Cary Bio 300 with Cary/Varian Peltier temperature control). The amount of dissolved drug was quantitated using the response of a drug standard solution. The incubated suspension A was also filtered through a 0.22 μm filter, the supernatant was quantitatively diluted with 50:50 water:methanol, and the dissolved drug quantitated versus the standard solution. To determine the effect of polymer concentration on drug solubility (hydroxypropylcellulose), both the ensemble methods above were applied to suspension E in dissolution media of 1%, 3%, and 4.3% polymer at 37 °C.

### 2.3. Diffusion coefficient

The diffusion coefficient for the drug was measured by the method of stopped time (diffusive) migration (Terabe et al., 1991; Yao and Li, 1994). A 0.4 mg/mL sample plug was transported to the center of the capillary via an electric field of 20 kV, the electric field set to zero for an incubation time chosen by the user, then returned to 20 kV. The UV absorbance chromatogram was exported to a suitable computer program; a linear least squares fit to a Gaussian function determines the peak variance. At least three injections were recorded for each chosen stop time.

### 2.4. Dissolution media viscosity

The viscosities of the dissolution media containing 1%, 3%, and 4.3% polymer were determined by recording the shear stress over a shear rate range of 1–1000 $s^{-1}$. The temperature of the

medium during the measurement was maintained at 37 °C by a Peltier plate (TA Instruments AR 2000).

### 2.5. Powder dissolution rates

Experimental powder dissolution rates, $\dot{\mu}_{EXP}$, were acquired by recording the absorbance as a function of time for the $D_{(solid)} \rightarrow D_{(aqueous)}$ transition using an optical fiber dip probe (C Technologies, Cary 50) immersed into standard Type II dissolution vessels (Van Kel 7010). The dissolution medium was 900 mL of the suspension stabilizing solution (i.e. water with 1% polymer and about 1/10th of a percent surfactant, w/w) maintained at 37 ± 0.3 C. With the paddle rotating at the desired frequency (50 rpm) and the dissolution medium at the experimental temperature, 1.00 mL of the suspension was manually injected into the dissolution vessel with an electronic pipette. In the suspension sample, less than 0.1% of the drug was in the dissolved state. At 50 rpm, there was no observed settling.

The injection contains 5% or less of the mass required to saturate the dissolution vessel, therefore all powder dissolution experiments were recorded under sink conditions. The dip probe, of optical path 1 cm, was electronically sampled at approximately 1 Hz to record the powder dissolution kinetics. The terminal absorbance for the experiment was approximately 0.2.

### 2.6. Dissolution instrument function and rate limiting process

Quantitating static or interfacial properties via decomposition of the experimentally recorded powder dissolution rate $\dot{\mu}_{EXP}$ into component amplitudes and rates requires delineation of at least three rates: (1) $\dot{\mu}_{MIX}$, the rate at which the particle centers of mass are dispersed throughout the dissolution volume. This mixing rate does not describe the transfer of mass from the solid to the aqueous state, (2) $\dot{\mu}_{SOL}$, the transfer of mass from the interfacial solid surface into the saturated band of the diffusion boundary layer, and (3) $\dot{\mu}_{TRANS}$, the mass transport rate, describes the mass flow from the saturated aqueous band, across the diffusion boundary layer, to a distance $h_{EFF}$ along the surface normal. Theoretical analysis and interpretation of the experimentally recorded powder dissolution data $\dot{\mu}_{EXP}$ is possible when it can be demonstrated which of $\dot{\mu}_{MIX}$, $\dot{\mu}_{SOL}$, or $\dot{\mu}_{TRANS}$ is the limiting rate.

The instrument function $\dot{\mu}_{MIX}$ was measured by performing the identical suspension dissolution procedure, substituting a true solution of chromophore for the suspension sample. Note under these conditions $\dot{\mu}_{SOL}$ and $\dot{\mu}_{TRANS}$ are infinitely fast, therefore $\dot{\mu}_{MIX}$ is the limiting rate, which is recorded as $\dot{\mu}_{EXP}$.

To determine which of $\dot{\mu}_{SOL}$ or $\dot{\mu}_{TRANS}$ is the limiting rate in the experimental powder dissolution rate, $\dot{\mu}_{EXP}$ was acquired for suspension E over a range of dissolution medium viscosities. Suspension E was chosen because it is the best characterized suspension, and as a suspension with one of the smallest particle size, predicted to have one of the smallest diffusion boundary layers.

The experimental powder dissolution rates, $\dot{\mu}_{EXP}$, were acquired in dissolution media of viscosities of 2.7, 10.0, and 20.0 cP (37 ± 0.3 °C) by varying the weight percent of the stabilizing polymer from 1% to 4.3%. The instrument function time constants for $\dot{\mu}_{MIX}$ were also determined as discussed above for each dissolution medium viscosity.

## 3. Results

### 3.1. Particle size distributions and surface area

The mean and standard deviations of the particle size distributions results are given in Table 1, complete mass distributions are shown in Fig. 1. The mass distributions in Fig. 1 are not instrument limited with respect to diameter; the instrument has

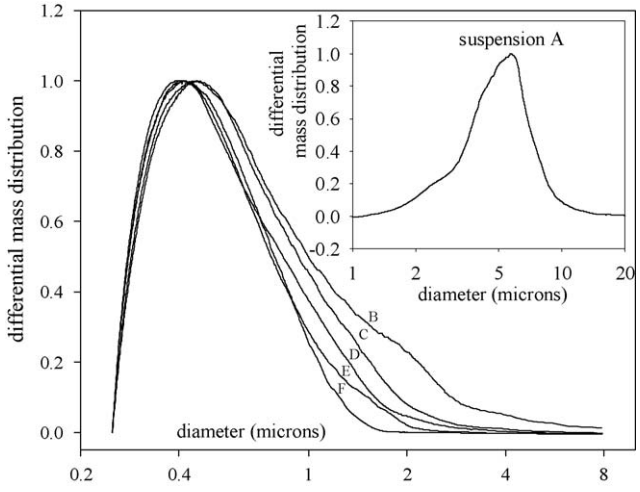


Fig. 1. Differential centrifugal sedimentation particle size distributions for suspensions A through F. Note log abcissa; distributions height normalized. *Inset*: Suspension A. (Right to left) Suspensions B, C, D, E, F. The distributions in this figure are single injections. Four to seven injections were recorded for each suspension. The result means and standard deviations are reported in Table 1.

Table 1
Fundamental data and calculation results for the determination of the diffusion boundary layer width $h_{EFF}$

| Suspension | Diameter [vol, 50%] (μm) | Specific surface area ($m^2$/g) | Dissolution time constant, $\tau_{50}$[a] (s) | Solubility at 37 °C (μg/mL) | Effective diffusion boundary layer, $h_{EFF}$ (μm) |
|---|---|---|---|---|---|
| A | 5.9 ± 0.10 | 0.21 ± 0.005 | 2426 ± 5 | 46 ± 8 | 8.5 ± 1.9 |
| B | 1.0 ± 0.10 | 1.34 ± 0.08 | 63 ± 6 | 47 ± 5 | 1.4 ± 0.4 |
| C | 0.73 ± 0.02 | 1.65 ± 0.04 | 28 ± 1 | 46 ± 5 | 0.80 ± 0.18 |
| D | 0.64 ± 0.08 | 1.69 ± 0.18 | 20 ± 6 | 50 ± 6 | 0.60 ± 0.21 |
| E | 0.56 ± 0.07 | 1.79 ± 0.16 | 11 ± 6 | 60 ± 6 | 0.44 ± 0.19 |
| F | 0.53 ± 0.05 | 2.00 ± 0.08 | 6 ± 1 | 77 ± 8 | 0.34 ± 0.14 |

[a] Instrument function time constant $\tau_{50}$ for 1% polymer dissolution medium at 37 °C = 7 ± 1 (s).

demonstrated the ability to record mass distributions centered at 10 nm. The mass homogeneity with respect to diameter is demonstrated by a full width at half maximum/diameter [volume, 50%] value of less than 0.7 for suspensions A through F.

As particle size distribution results can be method biased, the differential centrifugal sedimentation results were verified by a near orthogonal, ensemble method. Multiangle light scattering with polarization intensity differential scattering (Coulter LS230) was used to challenge the differential centrifugal sedimentation results. Good agreement was observed between the methods.

For each suspension, means and standard deviations for specific surface area are shown in Table 1. Note this is not the Angstrom scale specific surface area as measured in a gas sorption experiment: the surface area of interest here is the area accessible to a high surface tension fluid such as water at atmospheric pressure.

### 3.2. Powder solubility

The drug solubilities of suspensions A through F clarified via ultracentrifugation and measured via HPLC analysis of the supernatant are tabulated in Table 1. The two ensemble methods for suspension A are in good agreement with each other, and with the solubility measurements via ultracentrifugation and HPLC analysis. The means of the method results were within 20%. The drug solubility for suspension E in the dissolution media containing 3% and 4.3% polymer were indistinguishable from the results obtained in the dissolution media containing 1% polymer, i.e. over this concentration range, the hydroxypropylcellulose had no observable effect on the drug solubility.

### 3.3. Diffusion coefficient

The plot of the variances versus stopped time was analyzed to extract an aqueous diffusion coefficient of $(0.75 \pm 0.1)\text{e}{-5}\ \text{cm}^2/\text{s}$ (Fig. 2).

### 3.4. Dissolution medium viscosities

Three to five determinations were recorded for each medium; all media displayed strongly Newtonian responses over this frequency range. The mean and standard deviations calculated from the multiple viscosity determinations are reported in Table 2.

### 3.5. Powder dissolution rates

An exponential rise to a maximum function was fit to the experimentally recorded data points to extract the initial, linear rate from the dissolution data. This linear rate, $\dot{\mu}_{\text{EXP}}$, was determined for each injection of each suspension. Three to seven dissolution trials were conducted for each suspension (see Fig. 3). In some instances, to obtain reasonable determinations of the initial, linear dissolution rate, biexponential functions were required to obtain satisfactory fits; no attempt was made to assign physical content to amplitude parameters.

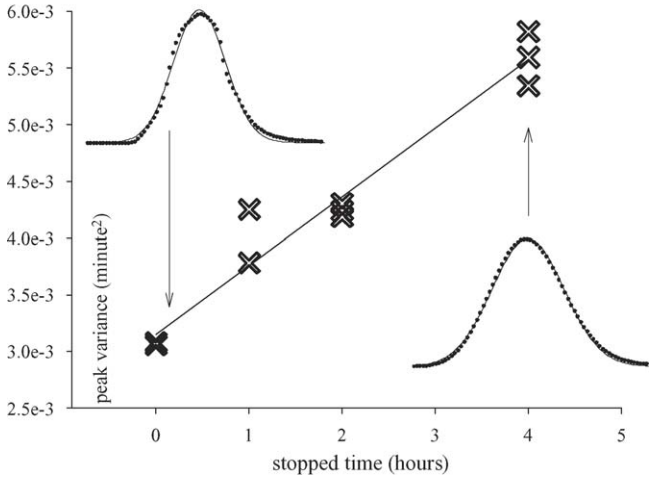


Fig. 2. Diffusion coefficient via stopped time capillary electrophorises. (Solid circles) Data points acquired via capillary electrophoresis with UV absorbance detection. (Solid lines through solid circles) Gaussian least squares fit to data points. (Black crosses) Peak variances obtained from Gaussian fits. (Solid line through crosses) Linear least squares fit to crosses to determine diffusion coefficient.

In addition to the traditional unit weight fitting matrix, a weighting scheme of $1/y^2$ ($y$, absorbance) was conducted to emphasize the earliest experimental data points at the expense of the latter. The time constants extracted via the $1/y^2$ weighting are statistically indistinguishable from those acquired via the unit weighting; an analysis of the total residuals and the residuals in the vicinity of interest could not recommend one weighting scheme over the other. Another approach to rate extraction, a linear fit to the dissolution data points for fraction dissolved of about 0.7 and less, yield very similar numerical values to exponential fitting with subsequent determination of initial, linear rates. For

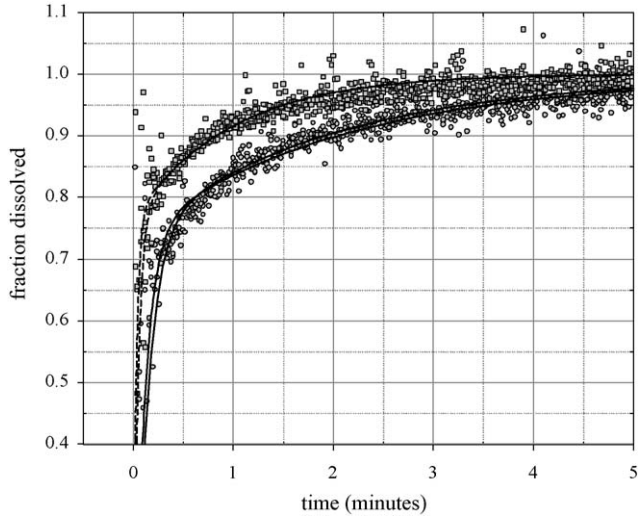


Fig. 3. Powder dissolution kinetic data and fits. (Gray squares) Experimental data points, two trials of suspension C. (Dashed black lines) Least squares fits to suspension C experimental dissolution data. (Grey circles) Experimental data points, two trials of suspension B. (Solid black lines) Least squares fits to suspension B experimental dissolution data. Mean dissolution times from multiple trials for suspensions A through F are reported in Table 1.

Table 2
Viscosity variation shows that dissolution kinetics are diffusion limited

| Suspension | Diameter [vol, 50%] (μm) | Weight polymer (%) | Viscosity at 37 °C (cP) | Dissolution time constant $\tau_{50}$ (s) | Instrument time constant $\tau_{50}$ (s) |
|---|---|---|---|---|---|
| E | 0.56 ± 0.07 | 1 | 2.7 ± 0.3 | 11 ± 6 | 7 ± 1 |
| | | 3 | 10.0 ± 0.3 | 23 ± 5 | 8 ± 2 |
| | | 4.3 | 20.0 ± 2.0 | 79 ± 52 | 11 ± 5 |

an extracted rate constant, no correlation was observed between the fitting protocol and the particle size of the suspension, so there was no apparent systematic bias. The magnitude of the dissolution rate scatter from different fitting protocols of a given dissolution trial was about the same as observed using a fixed fitting protocol across multiple trials of a given suspension. All correlation coefficients for retained time constants are >0.90, most are >0.96.

For suspensions A through F, 3–10 powder dissolution trials were conducted for each suspension. The experimental dissolution rates are most conveniently tabulated and compared as time constants. Recall that the mass transfer rates of interest here are the initial, linear rates, of a single chemical compound under sink conditions. In zeroth-order kinetics, the time constant and the rate constant are inversely related. The dissolution times reported are $\tau_{50}$, the time required to dissolve 0.5 of the drug mass. The means and standard deviations for each suspension are reported in Table 1.

### 3.6. Dissolution instrument function and rate limiting process

At least three trials of red food dye dissolved in stabilizer solution were recorded for each dissolution condition. For each trial, the initial, linear rate was extracted using a fitting procedure identical to the one used for analysis of the suspension dissolution. The time constant for the instrument function, $\tau_{50}$, has the same definition as for dissolution time for suspensions A through F: the time required for the absorption to attain 0.5 of its terminal value. For the 1% polymer by weight dissolution medium, the instrument function time constant mean and standard deviation is reported in Table 1. An inspection of Table 1 shows that the dissolution times of suspensions A through E are longer or about equal to the instrument function time constant 7 ± 1 s. Therefore, $\dot{\mu}_{MIX} > \dot{\mu}_{EXP}$, and the experimentally recorded dissolution data and time constants for these suspensions are recording the dissolution kinetics.

At least three dissolution trials of both suspension E and dye solution were conducted for each viscosity; the means and standard deviations are reported in Table 2. An inspection of Table 2 shows that the dissolution time $\tau_{50}$ for suspension E increases as the dissolution medium viscosity increases. Note the approximate 7×-fold increase in viscosity (2.7 ± 0.3 to 20 ± 2.0 cP) results in a corresponding 7×-fold increase in dissolution time for suspension E; recall the Stokes–Einstein diffusion coefficient is inversely proportional to the viscosity. This linear correlation between $\tau_{50}$ and medium viscosity is observed over the entire experimental viscosity range; a linear regression analysis of suspension E $\tau_{50}$ versus medium viscosity results in a slope of 3.99 s/cP, with a correlation coefficient of 0.97. The experimentally recorded $\dot{\mu}_{EXP}$ is recording a diffusion limited process.

### 3.7. Expression to evaluate $h_{EFF}$ via diffusion expression

Differential analysis of diffusion kinetics have been the subject of scientific inquiry since Fourier (1807, 1822), modified by Fick (1855), Noyes and Whitney (1897), and Nernst (1904), and to yield the familiar expression:

$$\dot{\mu}(t) = \beta(d;t) \times D \times A_{INT}(t) \times \frac{C_{SAT} - C_{\infty}(t)}{h_{EFF}}, \quad (1)$$

where $\dot{\mu}(t)$ is mass diffusion rate of the drug from the solid state to the infinite fluid; because the experimental dissolution rate $\dot{\mu}_{EXP}$ is recording a diffusion controlled mass transfer process, $\dot{\mu}_{EXP}$ can be set equal to equation (1). $\beta$ is the unitless mass transfer coefficient describing the hydrodynamic coupling between the drug powder and the fluid, $D$ is the diffusion coefficient of the solute, $A_{INT}(t)$ is the interfacial area of the drug powder, i.e. the area of the powder in contact with the dissolution medium providing mass flux from the powder to the fluid. The concentration gradient $C_{SAT} - C_{\infty}(t)/h_{EFF}$ is formed by the high concentration $C_{SAT}$, observed within the hydrodynamic boundary layer at the solid–liquid "wall", decreasing to $C_{\infty}(t)$, observed in the fluid at distance $h_{EFF}$ and greater from the powder surface.

With respect to the powder shape variation across the suspension series, recall powders A through F have been processed in an attempt to form narrow, homogeneous distributions of isotropic spheres. Optical microscopy of suspension A and ESEM of suspension E show remarkably homogenenous distributions of spherical powders. These qualitative observations are substantiated by narrow time of flight distributions observed in the sedimentation data (Fig. 1). Given these results, and given that suspension A through F have indistiguishable PXRD diffractograms, no attempt is made in Eq. (1) to assign unique shape factors to each suspension.

The coupling $\beta$ between the suspended particle and the agitated fluid is a strong function of $d$, the particle diameter. If the hydrodynamic coupling between the particles and the dissolution medium is suspension specific, to extract the effective diffusion boundary layer the experimentally recorded dissolution rates $\dot{\mu}_{EXP}$ have to be appropriately scaled by using a unique value of $\beta$ for each suspension. The particles in suspensions A through E are <6 μm (suspension A diameter [volume, 50%] = 5.9 ± 0.1 μm), have negligible Reynolds and Schmidt numbers, and the Sherwood number may be taken as 2 (Harriott, 1962; LeBlanc and Fogler, 1987). At this hydrodynamic

coupling, the ensembles are all in the no slip limit, i.e. follow the fluid exactly (Friedlander, 1957; Bocanegra et al., 1990). All ensembles transfer mass with the same efficiency, and $\beta$ can be set to 1 for all suspensions. While at first glance it may seem that some of the mass of suspension A could be outside the no slip limit, for clarity of analysis, the suspensions initially will be considered to have equal mass transfer coefficients. The validity of this model choice is addressed in the Section 4, below.

The powder dissolution rate $\dot{\mu}_{EXP}$, is the initial, linear rate in which half the injected mass $\mu_0$ dissolves in the time $\tau_{50}$. The powder dissolution data was acquired under sink conditions, where $C_\infty(t) \ll C_{SAT}$, and Eq. (1) is rearranged:

$$h_{EFF} = \frac{2\tau_{50} D \times A_{INT}(t) \times C_{SAT}}{\mu_0} \quad (2)$$

For an ensemble of spheres such as suspensions A through F for the time period $t = 0$ to $\tau_{50}$, in which the mass or volume decreases linearly with time, the surface area $A_{INT}(t)$ decreases as $t^{2/3}$. Although the interfacial area $A_{INT}(t)$ does not decrease greatly over the time period of interest, the average value $\langle A_{INT}(t) \rangle$ can be calculated in a straightforward manner (see Appendix A) to yield:

$$h_{EFF} = 1.6\tau_{50} \times D \times \hat{S} \times C_{SAT} \quad (3)$$

where $\hat{S}$ is the initial specific surface area of the suspension (Table 1). Because $A_{INT}(t)$ is averaged over time, equation (3) yields a time averaged value for $h_{EFF}$. After the Stokes–Einstein calculation to adjust the measured diffusion coefficient to the dissolution medium viscosity, the effective diffusion boundary layer $h_{EFF}$ is determined for suspensions A through F using Eq. (3); the results are tabulated in Table 1, and plotted in Fig. 4. The uncertainties for $h_{EFF}$, listed in Table 1 and plotted in Fig. 4, are calculated via standard propagation of error analysis (Shoemaker et al., 1996); the uncertainties used for $t_{50}$, $D$, $\hat{S}$, and $C_{SAT}$ are those listed in Table 1 and elsewhere, i.e. one standard deviation. The $h_{EFF}$ reported in Table 1 may be interpreted as identifiable with 50 rpm. This gentle stirring is applicable to biodissolution, and therefore pharmaceutical program development.

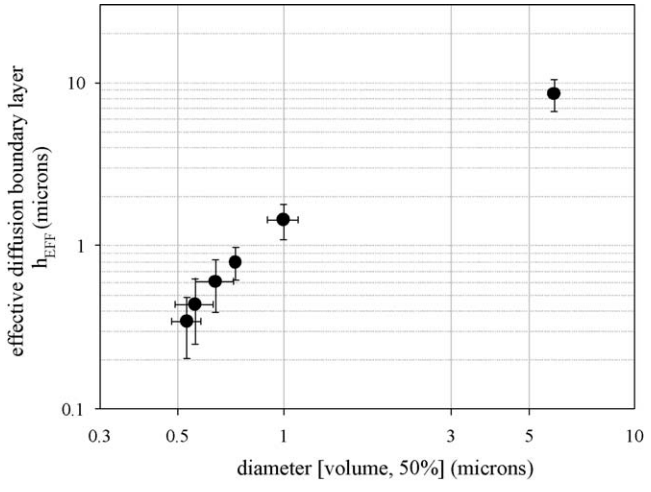


Fig. 4. Experimentally determined values for the effective hydrodynamic diffusion layer $h_{EFF}$. (Black solid circles) $h_{EFF}$ calculated for suspensions A through F by evaluation of equation (3) using data tabulated in Table 1. Error bars for $h_{EFF}$ calculated using standard propagation of error analysis; uncertainties used for $t_{50}$, D, $\hat{S}$, and $C_{SAT}$ are those listed in Table 1 and elsewhere, i.e. one standard deviation.

## 4. Discussion

For suspensions A through F, the experimentally determined effective diffusion boundary layer $h_{EFF}$ ranges from a $h_{EFF}/d_{50}$ value of 1.4 for suspension A to 0.64 for suspension F (Table 1 and Fig. 4). In the small particle regime, $d_{50}$ less than about 50 μm, the use of the particle radius or diameter as the effective diffusion boundary layer to calculate powder dissolution rates (Hintz and Johnson, 1989) is justified, and is a tremendous improvement over the use of a fixed $h_{EFF}$ of 30 μm. As a property of the interfacial solid–fluid structure, resulting from the small surface area per particle, this observation can be expected for all mass diffusion controlled transport, i.e. not compound or compound class specific. Note the so-called "intrinsic dissolution rate" can only exist in regimes where $h_{EFF}$ is a constant property of the powder.

Understanding the mechanics of mass transport as a function of particle size is important for scientists who wish to avoid unnecessary thermodynamic ensemble instability. A high value target in this design area is the largest particle size that moves the dosage form from solubility limited to permeability limited. Recall we have previously noted that in regimes where $h_{EFF}$ is constant, e.g. in the large particle regime of diameter greater than about 50 μm, the dissolution rate is proportional to the specific surface area, and varies as $d^{-1}$. As the particle size decreases through the small particle regime, because $h_{EFF}$ is approximately equal to the particle radius or diameter, the dissolution rate in this regime should increase as $d^{-2}$. A log–log plot of dissolution time versus diameter over the small particle regime for this model is predicted to have a slope of 2; this theoretical line is plotted as gray squares and gray dotted line in Fig. 5. The

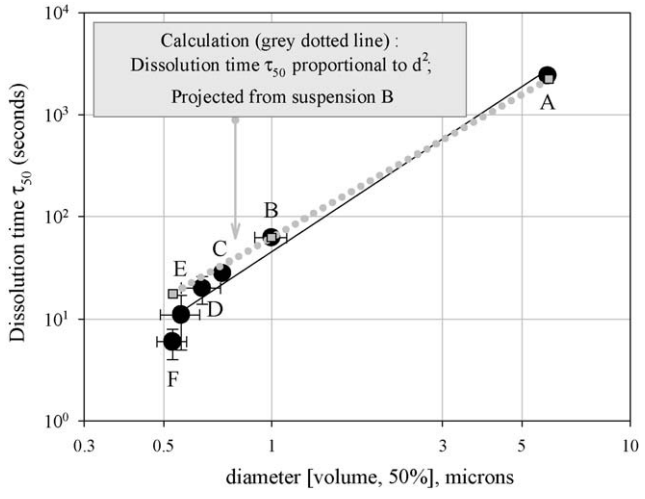


Fig. 5. (Black solid circles) Experimental dissolution time $\tau_{50}$ versus $d_{50}$ from Table 1. (Black solid line) linear least squares fit to experimental data. $R^2 = 0.98$, slope = 2.3. (Gray squares and gray dotted line) Calculated dissolution time proportional to $d^2$ ($d$ = diameter), slope = 2.0.

experimental results for suspensions A through F dissolution time versus diameter are plotted as black circles in Fig. 5; the solid black line is a linear least squares fit to the experimental data (slope = 2.3, $R^2 = 0.98$), which is in good agreement with the theoretical expectation of a slope of 2. The transformation of the dissolution rate from proportional to $d^{-1}$ to proportional to $d^{-2}$ as the particle size decreases should be clearly understood by pharmaceutical scientists.

Typically, a pharmaceutical development program of a poorly soluble drug has a powder diameter, the corresponding in vivo or in vitro release profile, and a desired p$K$ target. The task is to calculate the particle size of the most stable ensemble which still achieves the desired dissolution rate. For example, to increase the dissolution rate of suspension A by a factor of 10×, it is not necessary to increase the specific surface area by a factor of 10× by decreasing the particle diameter to 0.59 μm. The work of cohesion required for this particle size reduction is stored as destabilizing surface energy. If the powder in suspension A has a specific surface energy of $\hat{G}_{\mathrm{SURFACE}}$, the 0.59 μm ensemble is unstable with respect to suspension A by 10 $\hat{G}_{\mathrm{SURFACE}}$. As shown in Figs. 4 and 5, however, a 10-fold increase in the dissolution rate of suspension A can be achieved by a diameter reduction to about 1.9 μm, because this size reduction increases the specific surface area of suspension A by $10^{1/2}$, and decreases the effective diffusion boundary layer by $10^{1/2}$. The 1.9 μm ensemble has $10^{-1/2}$ the specific surface area of the 0.59 μm ensemble, and therefore has only $10^{1/2}$ $\hat{G}_{\mathrm{SURFACE}}$ work of cohesion stored as a destabilizing Gibbs energy with respect to suspension A. The 1.9 μm ensemble, as the most stable powder ensemble which achieves the required dissolution rate, is the high value target.

Although the agreement between the theoretical value of the slope and the experimentally obtained value in Fig. 5 is quite good, there is evidence of some negative curvature which warrants discussion. One might hypothesize that the dissolution time of suspension A is depressed from expectation because it contains mass which slips in the dissolution fluid, increasing interfacial friction and thereby decreasing dissolution time from expectation. However, suspension A dissolution time is collinear with suspensions B, C, and D, and the line comprised by these dissolution times has a slope very close to two, in good agreement to the Prandtl theoretical expectation. It seems more likely that the curvature in the $\tau_{50}$ versus $d_{50}$ data results from *faster* dissolution rates for suspensions F and E than predicted by the dissolution time proportional to diameter squared model.

The curvature of the $\tau_{50}$ versus $d_{50}$ data is consistent with the solubility versus suspension particle size data, which also shows a sharp deviation from the linear regime at $d_{50}$ about 0.6 μm (see Fig. 6). The $\tau_{50}$ for suspensions F and E lie below the dissolution time proportional to diameter squared line because that model does not include changes in solubility. Introducing solubility in the model significantly decreases the data curvature: fitting $\log(\tau_{50} \times \text{solubility})$ versus $\log(d_{50})$ reduces the diameter exponent to $\tau_{50} \times$ solubility proportional to diameter$^{2.2}$ and increases the correlation ($R^2 = 0.99$), at the expense of some model transparency.

The experimentally observed increase in solubility of about 70% over this suspension series (Table 1, Fig. 6) is significantly larger than the approximately 2% predicted by the LaPlace–Young–Kelvin expression (e.g. Muller and Peters, 1998). Note, however, there are serious objections to the application of the LaPlace–Young–Kelvin expression to organic solid–solute equilibria (Wu and Nancollas, 1998, and references therein). Regarding the possibility of high energy polymorphs or amorphous content, while no evidence was observed in the PXRD diffractograms of the suspension series, due to the low sensitivity of the method, this scattering data cannot rule out the presence of a low level, amorphous impurity in suspensions E and F. For instance, the ultrahigh pressure homogenization may increase the structural defect density of the particles. The cause of the solubility increase of suspensions E and F is of interest, and may be investigated by higher sensitivity methods such as isothermal and scanning calorimetry. The measured solubility difference over the suspension series does not interfere with the experimental determination of $h_{\mathrm{EFF}}$.

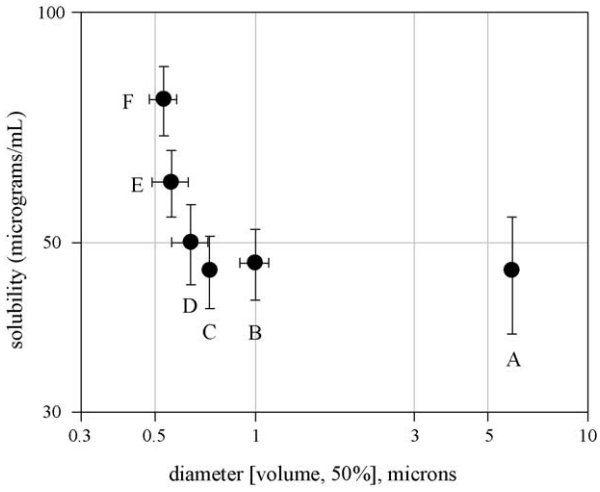


Fig. 6. (Black solid circles) Experimental powder solubility versus $d_{50}$ from Table 1. Note log–log scaling. Solubility measured via incubation at 37 °C, ultracentrifugation, supernatant dilution, and HPLC analysis; four to six trials completed for each suspension. Error bars: one standard deviation about mean.

While the experimentally determined $h_{\mathrm{EFF}}$ in suspension series A through F is in good agreement with Prandtl theory ($h_{\mathrm{EFF}}/d_{50}$ suspension series mean ± standard deviation = 1.0 ± 0.3), it is interesting to note that $h_{\mathrm{EFF}}/d_{50}$ is a slightly increasing function of $d_{50}$: the quantity $h_{\mathrm{EFF}}/d_{50}$ increases from about 0.64 for suspension F to 1.4 for suspension A. The correlation between $h_{\mathrm{EFF}}/d_{50}$ and $d_{50}$ may be related to the evolution of the particle size distribution to a more symmetric function as the processing time increases. Also, considering the surface interactions between the stabilizing excipients and the particles, the correlation may reflect specific hydrodynamic properties such as compressibility. Dissolution rates as a function of paddle speeds could provide a window on the excipient compressibility over a series like suspension A through F.

An interesting product of the investigation herein is the understanding that because the dissolution time is proportional to the square of the diameter in the small particle regime, the analytical discrimination between ensembles via powder dissolution is quite high, e.g. significantly higher than traditional ensemble

particle size methods such as photon correlation spectroscopy or Mie scattering, and also higher than methods using separation prior to quantitation, such as differential centrifugal sedimentation. Powder dissolution, the performance based analysis, not only probes the specific biopharmaceutical properties of interest, it does so with enhanced discrimination.

## 5. Conclusion

This work has shown that for ensembles in the small particle regime (six suspensions over the particle diameter range of $5.9 \pm 0.1$ to $0.53 \pm 0.05$ μm [volume, 50%]), the effective diffusion boundary layer $h_{EFF}$ is approximately equal to the particle radius or diameter. As a consequence, the dissolution times in this regime are expected to be proportional to $d^{2.0}$; the experimental results of dissolution time proportional to $d^{2.3}$ are in good agreement with this expectation. Understanding the mechanics of diffusion transport in both the large particle and small particle regime enables the pharmaceutical scientist to design dosage forms with the required dissolution profile, while avoiding unnecessary ensemble instability.

## Acknowledgements

The author would like to acknowledge frequent and rewarding discussions with Dr. Bruce Johnson, both before, during and after the experimentation. These discussions brought many key issues into scientific focus. Dr. Johnson also greatly improved an early draft of this manuscript with his thoughtful criticism and editing skill. The author is deeply in his debt. Dr. Brian Weekley and Dr. Peter Angus were very generous with their expertise and time regarding the measurements of the diffusion coefficient.

## Appendix A. Time average of the interfacial area $A_{INT}(t)$

Recall the linear decay of mass or volume:

$$V(t) = \frac{\mu_0}{\rho}\left(1 - \frac{t}{2\tau_{50}}\right)$$

where $\mu_0$ has been previously defined as the injected mass for powder dissolution. One half the mass, of density $\rho$, dissolves in time $\tau_{50}$. The interfacial area decays as the volume decay raised to the 2/3 power, where, at time = 0, the interfacial area equals the specific surface area $\hat{S}$ times the initial mass:

$$A_{INT}(t) = \hat{S}\mu_0\left(1 - \frac{t}{2\tau_{50}}\right)^{2/3},$$

The average value of the interfacial area over the time period $\tau_{50}$ is $\langle A_{INT}(t)\rangle$ and is calculated:

$$\langle A_{INT}(t)\rangle = \frac{\hat{S}\mu_0 \int_0^{\tau_{50}} (1 - (t/2\tau_{50}))^{2/3}}{\tau_{50}} = 0.82\hat{S}\mu_0$$

and substituted directly into Eq. (2) to yield Eq. (3).

## References

Bird, R.B., Stewart, W.E., Lightfoot, E.N., 1960. Transport Phenomena. John Wiley and Sons, New York.

Bisrat, M., Anderberg, E.K., Barnett, M.I., Nystroem, C., 1992. Physicochemical aspects of drug release. XV. Investigation of diffusional transport in dissolution of suspended, sparingly soluble drugs. Int. J. Pharm. 80, 191–201.

Bocanegra, L.M., Morris, G.J., Jurewicz, J.T., Mauger, J.W., 1990. Fluidity and particle laser Doppler velocity measurements and mass transfer predictions for the USP paddle method dissolution apparatus. Drug Dev. Ind. Pharm. 16, 1441–1464.

Carstensen, J.T., 1977. Pharmaceutics of Solids and Solid Dosage Forms. Wiley, New York.

Dali, M.V., Carstensen, J.T., 1998. Particle size distributions from multiparticulate dissolution. Drug. Dev. Ind. Pharm. 24, 637–644.

Fick, A., 1855. Ueber diffusion (on diffusion). Ann. Phys. Chem. J.C. Pogendorff 94, 59–86.

Fitzpatrick, S.T., 1999. Particle size analysis by differential centrifugal sedimentation. Advantages and limitations, recent progress, and future trends. Polym. News 24, 42–50.

Fourier, J.P.J., 1807. Theorie des mouvements de la chaleur dans le corps solides. French Academy, Paris.

Fourier, J.P.J., 1822. Theorie Analytique del la Chaleur (Theory of Heat). F. Didot, Paris.

Friedlander, S.K., 1957. Behavior of suspended particles in a turbulent fluid. AIChE J. 3, 381–385.

Galli, C., Lodaya, M., Mollan, M., Polack W., Shah, U., Vemaverapu, C., 2005. p*K* targeting via modular high pressure processing control: Novel formulation and characterization in the 10 micron to 100 nanometer range. Formulations/Preformulations Strategies Barnett BI-455CP, Philadelphia.

Grau, M.J., Kayser, O., Muller, R.H., 2000. Nanosuspensions of poorly soluble drugs-reproducibility of small scale production. Int. J. Pharm. 196, 155–159.

Grijseels, H., Crommelin, D.J.A., De Blaey, C.J., 1981. Hydrodynamic approach to dissolution rate. Pharm. Week. 116, 129–144.

Harriott, P., 1962. Mass transfer to particles. I. Suspended in agitated tanks. AIChE J. 8, 93–101.

Hendriksen, B.A., 1990. Characterization of calcium fenoprofen. 1. Powder dissolution rate and degree of crystallinity. Int. J. Pharm. 60, 243–252.

Hintz, R.J., Johnson, K.C., 1989. The effect of particle size distribution on dissolution rate and oral absorption. Int. J. Pharm. 51, 9–17.

Kitamori, N., Iga, K., 1978. Dissolution of nonspherical powders. J. Pharm. Sci. 67, 1674–1676.

LeBlanc, S.E., Fogler, H.S., 1987. Population balance modeling of the dissolution of polydisperse solids: rate limiting regimes. AIChE J. 33, 54–63.

Liversidge, G.G., Cundy, K.C., 1995. Particle size reduction for improvement of oral bioavailability of hydrophobic drugs. I. Absolute oral bioavailability of nanocrystalline danazol in beagle dogs. Int. J. Pharm. 125, 91–97.

Lu, A.T.K., Frisella, M.E., Johnson, K.C., 1993. Dissolution modeling: factors affecting the dissolution rates of polydisperse powders. Pharm. Res. 10, 1308–1314.

Merisko-Liversidge, E., Liversidge, G.G., Cooper, E.R., 2003. Nanosizing: a formulation approach for poorly-water-soluble compounds. Eur. J. Pharm. Sci. 18, 113–120.

Mosharraf, M., Nystroem, C., 1995. The effect of particle size and shape on the surface specific dissolution rate of microsized practically insoluble drugs. Int. J. Pharm. 122, 35–47.

Muller, R.H., Jacobs, C., Kayser, O., 2001. Nanosuspensions as particulate drug formulations in therapy. Rationale for development and what we can expect for the future. Adv. Drug Deliv. Rev. 47, 3–19.

Muller, R.H., Peters, K., 1998. Nanosuspensions for the formulation of poorly soluble drugs. I. Preparation by a size-reduction technique. Int. J. Pharm. 160, 229–237.

Nernst, W., 1904. Theorie der Reaktionsgeschwindigkeit in Heterogenen Systemen. Z. Phys. Chem. 47, 52–55.

Niebergall, P.J., Milosovich, G., Goyan, J.E., 1963. Dissolution rate studies. II. Dissolution of particles under conditions of rapid agitation. J. Pharm. Sci. 52, 236–241.

Noyes, A., Whitney, W., 1897. The rate of solution of solid substances in their own solutions. J. Am. Chem. Soc. 19, 930–934.

Rasenack, N., Mueller, B.W., 2005. Poorly water-soluble drugs for oral delivery—a challenge for pharmaceutical development. Part I. Physico-chemical and biopharmaceutical background/strategies in pharmaceutical development. Pharm. Ind. 67, 323–326.

Schlichting, H., 1955. Boundary Layer Theory. McGraw-Hill, New York.

Shoemaker, D.P., Garland, C.W., Nibler, J.W., 1996. Experiments in Physical Chemistry, sixth ed. McGraw-Hill, New York.

Terabe, S., Shibata, O., Isemura, T., 1991. Band broadening evaluation by back-and-forth capillary electrophoresis. J. High Res. Chrom. 14, 52–55.

Vaughn, J.M., Gao, X., Yacaman, M.-J., Johnston, K.P., Williams, R.O., 2005. Comparison of powder produced by evaporative precipitation into aqueous solution (EPAS) and spray freezing into liquid (SFL) technologies using novel Z-contrast STEM and complimentary techniques. Eur. J. Pharm. Biopharm. 60, 81–89.

Wu, W., Nancollas, G.N., 1998. A new understanding of the relationship between solubility and particle size. J. Sol. Chem. 27, 521–531.

Yao, Y.J., Li, S.F.Y., 1994. Determination of diffusion coefficients by capillary zone electrophoresis. J. Chrom. Sci. 32, 117–120.